Supporting Information of

Highly Active Catalyst for CO_2 Methanation Derived from a Metal-Organic Framework Template

Renata Lippi, Shaun C. Howard, Hector Barron, Christopher D. Easton, Ian C. Madsen, Lynne J. Waddington, Christian Vogt, Matthew R. Hill, Christopher J. Sumby, Christian J. Doonan,* and Danielle F. Kennedy*

Contents

General considerations

All chemicals were used as provided by the manufacturer. Chemicals and respective suppliers: Zirconium Oxide nanoparticle (99+% ZrO_2 monoclinic, 40 nm, US3600) US Nano (USA), Charcoal activated powder R Grade LabServ (Australia), Methanizer packing 391160002 Agilent Technologies (Australia), ruthenium(III) cloride trihydrate ($RuCl_3 \cdot 3H_2O$) 99% PMO Pty Ltd (Australia), terephthalic acid 99% Acros Organics (Great Britain), dimethylformamide (DMF) 99.8% Merck Pty. Ltd. (Australia), zirconium chloride ($ZrCL_4$) 99.5% Sigma-Aldrich (Australia), hydrochloric acid (HCl) 32% Merck Pty. Ltd. (Australia), Pluronic® P-123 Sigma-Aldrich (Australia), Tetraethylorthosilicate (TEOS) 99% Merck Pty. Ltd. (Australia). Silicon Carbide (SiC) 99% 300-355 µm Beijing HWRK Chem Co., Ltd. (China). Water was deionized by reverse osmosis. All gases used were supplied by Coregas (Australia) including custom made mixtures: nitrogen (N4); Argon (N5); Helium (N5); Hydrogen (N5); 25% carbon dioxide with hydrogen balance; and 2.52% ethane, 2.82% ethene, 2.53% acetylene, 2.44% methane, 2.48% carbon dioxide, 2.53% carbon monoxide, 2.51% hydrogen with argon balance.

Syntheses Details

UiO-66

UiO-66 was synthesized according to Katz et al.[1] A 2 L Schott glass bottle was loaded with DMF (160 mL), $ZrCl_4$ (4 g) and 32% HCl (32 mL), the mixture was sonicated for 20 minutes. In a separate bottle, terephthalic acid was dissolved in DMF (320 mL) and then added to the $ZrCl_4$ solution. The bottle was sealed with a screw cap and placed in an oven at 80 °C for 20 hours. The resulting solid was isolated by vacuum filtration and it was washed with DMF (3x 300 mL) and ethanol (2x 300 mL). Subsequently, the solid was dried under vacuum for several hours. The synthesis of UiO-66 was confirmed by PXRD and TGA.

SBA-15

Mesoporous silica SBA-15 was synthesized according to the method of Cool et al.[2] In a 2 L round bottom flask, 1083 mL of water, 33 g of P123 and 166 mL of 4 M HCl solution were mixed using a mechanical stirrer for approximately 6 hours until complete dissolution. After resting for 16 hours, TEOS was added to the mixture and the solution was stirred at 452 rpm and 45 °C for 8 h. The resulting solution was let ageing in an oven at 80°C for 20 hours. The white solid phase formed after ageing was cooled down and recovered by filtering and washing it with deionized water (3x 200 mL). Next, the solid was dried at 60 °C for 20 h before being calcined in a Nabertherm muffle furnace at 500°C for 24 hours (heating at 1 °C/min, cool down at 2 °C/min). Before use, the material was crushed using a mortar and a pestle.

Ru/Support via IWI

In a typical experiment where the support was UiO-66, 1 wt% loading of Ru^0 in UiO-66 (**1Ru/UiO-66**) was achieved by the standard incipient wetness impregnation method of UiO-66 with an aqueous solution of $RuCl_3$. Finely ground UiO-66 solid (250 mg) was placed into an 8 mL glass vial and an aqueous $RuCl_3$ solution ($7.12 \cdot 10^{-5}$ M, 350 µL) was added followed by mixing of the resulting slurry to ensure that all the sample was in contact with the solution. The sample was dried in air at 80 °C to obtain **1Ru/UiO-66**. The same procedure was applied for different supports using the appropriate solution volume and concentration to yield the right loading as presented in Table S1. Different loadings of Ru on UiO-66 were achieved by using appropriate concentration of $RuCl_3$.

The UiO-66 water uptake for the IWI was defined empirically. The total pore volume of approximately 0.4 cm^3/g was considered for the impregnation at first, however simple visual inspection indicated that it was not enough to create a homogeneous slurry. To define the water uptake for the IWI known amounts of water were added to UiO-66 until a homogeneous slurry was formed. The resulting value was 1.38 mL water/g UiO-66.

Table S1: Details of quantities used during the IWI procedure for different support materials.

		For 1% Ru loading	
Support	Volume aqueous solution to support mass (mL/g)	$RuCl_3 \cdot 3H_2O$ solution concentration (g/mL)	$RuCl_3 \cdot 3H_2O$ solution concentration (mol/mL)
UiO-66	1.38	$1.88 \cdot 10^{-2}$	$7.12 \cdot 10^{-5}$
$pmZrO_2$	0.636	$4.07 \cdot 10^{-2}$	$1.54 \cdot 10^{-4}$
Activated Carbon (C)	0.636	$4.07 \cdot 10^{-2}$	$1.54 \cdot 10^{-4}$
SBA-15	0.636	$4.07 \cdot 10^{-2}$	$1.54 \cdot 10^{-4}$

UiO-66 precursor mix ($ZrCl_4$+H_2BDC)

The preparation of UiO-66 precursors mix $ZrCl_4$ and terephthalic acid ($ZrCl_4$+H_2BDC) was designed considering the molecular formula of UiO-66, $C_{48}H_{24}O_{30}Zr_6$, in order to achieve the equivalent amount and ratio of Zr:BDC in 100 mg of UiO-66 ($6.15 \cdot 10^{-5}$ mol UiO-66), 86 mg of $ZrCl_4$ ($3.96 \cdot 10^{-4}$ mol $ZrCL_4$) was mixed with 61 mg of H_2BDC ($3.96 \cdot 10^{-4}$ mol H_2BDC), for the sample with Ru (Ru/$ZrCl_4$+H_2BDC), 2.5 mg of $RuCl_3 \cdot 3H_20$ (1 mg of Ru, $10 \cdot 10^{-6}$ mol Ru) was added to the solid mixture, this amount was chosen to simulate the Ru composition in **1Ru/UiO-66** when using 100 mg of UiO-66. These samples were kept under N_2 before the catalytic testing. For catalysis testing approximately 30 mg of the precursor mix was used since this amount is equivalent to 20 mg of UiO-66.

Table S2: Synthesis details and hydrogen conversion for the samples compared in this study.

	Synthesis details				350 °C, 5 bar	350 °C, 5 bar
Precatalyst acronym	Support	Metal precursor	Metal loading (wt%)	Impreg. method[a]	X_{H2} (%)	SD_{XH2}[b]
UiO-66	UiO-66	-	0	-	0	-
1Ru/UiO-66	UiO-66	$RuCl_3$	1	IWI	96.0	2.9
Ru/pmZrO2	Pre-made ZrO_2 (monoclinic)	$RuCl_3$	1	IWI	38.0	9.2
Ru/C	Activated carbon	$RuCl_3$	1	IWI	26.3	2.6
Methanizer	SiO_2	Ni[c]	10-30	ND	59.6	2.6
Ru/SBA-15	SBA-15	$RuCl_3$	1	IWI	0[d]	-
$ZrCl_4$+H_2BDC	Dry mixture of solids	-	0	DM	0	-
Ru/$ZrCl_4$+H_2BDC	Dry mixture of solids	$RuCl_3$	1[e]	DM	0	-

[a]IWI: Incipient Wetness impregnation, ND: not disclosed, DM: solvent-free (dry) solid mixture; [b]Standard Deviation across isopressure periods; [c]Ni precursor not disclosed; [d] sample tested at 10 bar; [e]Equivalent to 1%**1Ru/UiO-66**

Thermogravimetric analysis (TGA)

The thermal analysis of 4 samples submitted were carried out using a Netzsch STA 449 F1 Jupiter with SiC furnace and S-type sensor. Samples were heated to 350 °C at a rate of 10°C/min under either 100% N_2 or 5% H_2 in N_2 purge gas at flowing rate of 40 mL/min. An empty alumina crucibles were run as blank for each method to correct for baseline. The STA analysis was initially run with an isothermal cycle for 5 min to allow the samples to equilibrate with the purge gas conditions. These sections are not shown in the thermograms.

A sample of UiO-66 was heated to 800 °C under N_2 to observe the full decomposition. This sample was evaluated using a Mettler Toledo TGA 2. UiO-66 (19 mg) was loaded into an empty alumina crucible heated to 800 °C at 10 °C/min under N_2 purge gas at flowing rate of 30 mL/min. the sample was allowed to equilibrate at 25 °C for 10 minutes before the analysis, this section is not shown in the thermogram.

Simultaneous Thermal Analysis (STA) was performed to evaluate the carbon content in the MOF-derived catalyst. After catalysis testing the used catalyst was loaded in an alumina pan and STA was performed in a Netzsch STA 449 F1 system fitted with a SiC Furnace and an S-type DTA sensor. The sample was heated to 1000°C at 10°C/min heating rate under Air purge gas 20 mL/min. An initial blank run was carried out to correct for the baseline. Evolved Gas Analysis (EGA) was performed with Pfeiffer Thermostar Quadrupole Mass Spectrometry coupled to the STA system in order to check for the volatiles.

Gas sorption analysis

The sample was degassed overnight at 150 °C. N_2 sorption was performed at 77 K using a Micromeritics ASAP 2020.

X-ray powder diffraction (XRD)

Laboratory source XRD

Where possible, samples were back-loaded into sample holders prior to the collection of XRD traces to minimize texture. Where insufficient sample was provided for back-loading, samples were instead loaded onto zero background plates. A Bruker D8 Advance X-ray Diffractometer operating under CuKα radiation (40kV, 40mA) equipped with a LynxEye detector was employed to obtain the XRD patterns. Samples were scanned over the 2θ range 3.5° to 130° with a step size of 0.02° and a count time of 0.4 second per step. 173/192 of the sensor strips on the LynxEye detector were used, to give an equivalent count time of 69.2 seconds per step.

Synchrotron source XRD (Gas controlled and variable temperature experiment)

Gas controlled and variable temperature XRD experiments were carried at the Powder Diffraction Beamline at the Australian Synchrotron. A Mythen microstrip detector[3] was used for data collection. The samples were loaded into open-ended special glass 0.7 mm wide capillaries (The Charles Supper Company, USA) glass wool was used to contain the powder within the capillary. The capillary was kept oscillating during acquisition. Temperature was controlled using a hot-air blower positioned below the capillary. The capillary holder was attached to a gas fitting, which was connected to a gas manifold allowing the selection of gas flow. The beam energy during data acquisition was 15 keV with a current of 200 mA. The sample was first heated to 220 °C under N_2 flow, then at 19 min, the gas flow was replaced with a mixture of CO_2:H_2 = 1:3. Upon reaching 350 °C, the temperature was kept constant.

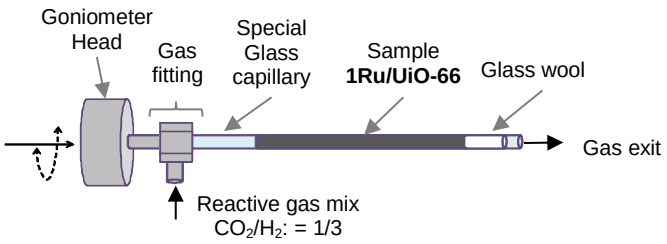

Figure S1: Gas controlled PXRD experiment sample holder setup.

Rietveld refinement of PXRD data

The quantitative phase and microstructure analysis of the laboratory source XRD data was performed using a whole-pattern, Rietveld based approach. The Rietveld method involves the development of a model which is used to generate a calculated XRD pattern. The model includes parameters such as crystal structure model for each phase, pattern background, wavelength, sample and instrument aberrations, etc. The then calculated pattern is compared with the observed data and the difference between observed and calculated is minimised through a least squares process by adjusting selected parameters in the model. These calculations were performed using the software TOPAS V5[4] in batch mode.

Synchrotron source was used for the gas controlled variable temperature PXRD of **1Ru/UiO-66**. Rietveld refinement of the scale UiO-66 and the resulting amorphous phase was performed in batch mode using Topas V5[4]. The Rietveld refinement of this XRD dataset was performed in batch mode starting with the diffractogram at 19min. The values refined for each diffractogram were used as input for the next. The background contribution for all diffractograms was fixed according to the refined values at 19min. Thereafter, the increase in the background was correlated with the generation of an amorphous phase.

Catalysis testing

Catalyst screening and optimization experiments were undertaken in a Flowrence® 48-channel catalysis rig manufactured by Avantium Ag.[5, 6] (**Figure S2**). The tubular reactors had internal diameters of 2.0 mm, were 280 mm long and were constructed of either Hastaloy with a stainless steel frit or quartz with a quartz frit depending on the experiment. Hastalloy reactors were prepared with a base of 700 mg of SiC to a height of 11-13 cm to maintain the catalyst bed within the isothermal zone of the reactor which is 8 cm in length. Precatalyst masses of between 10 and 20 mg were diluted with coarse SiC to produce a catalyst bed volume between 50 and 200 uL in each reactor. Quartz reactors were loaded with quartz frits and undiluted precatalysts (~50 mg). The reactors were operated in co-current downstream mode and can operate at a maximum temperature of 750 °C, a maximum pressure of 160 bar and GHSVs of up to 100,000 h^{-1}.

This multichannel reactor was custom built for CSIRO and is comprised of 3 blocks of 16 reactors which can be independently temperature controlled allowing the concurrently testing of samples at different temperatures. Pressure is maintained with 2 backpressure manifolds each lined with a Teflon membrane, the gas feed and pressure is kept even for all reactors. Flow rates are modulated by EL-Flow Bronkhorst mass flow controllers. Effluent gases were diluted with nitrogen immediately after exiting reactors to provide enough volume to the GC analytics. The tracing line between the reactors and the GC was maintained at 120 °C.

All reactors were sequentially sampled by an on-line Gas Chromatograph 7890A Agilent (USA). The complete effluent analysis consisted of two methods performed in parallel on two GC channels: Front channel with an Agilent PoraBOND Q packed column (CP7352) with a TCD detector; and Auxiliary channel with an Agilent MolSieve 5A packed column (G3591-80046) with a TCD detector with negative polarity. In both channels, helium was used as sweep gas. Argon was mixed with the gas feed (3 vol% of argon in feed) as an internal standard required to calculate absolute flows.

Before the beginning of the experiments, a validation run was carried out with a Alfa Aesar Cu–ZnO–alumina catalyst for methanol synthesis, to perform a technical validation of the equipment. During this validation, various process parameters were studied: temperature: 260 and 300 °C; pressure: 10, 20 and 30 bar; H_2/CO molar ratio: 0.5, 1 and 2; GHSV: 4000, 8000, 16,000 h^{-1}. As expected, as this catalyst was designed for H_2/CO operations the product mixture is complex. The main product in this reaction was methanol. The data from this validation run showed that the equipment is capable of producing consistent and reproducible data.

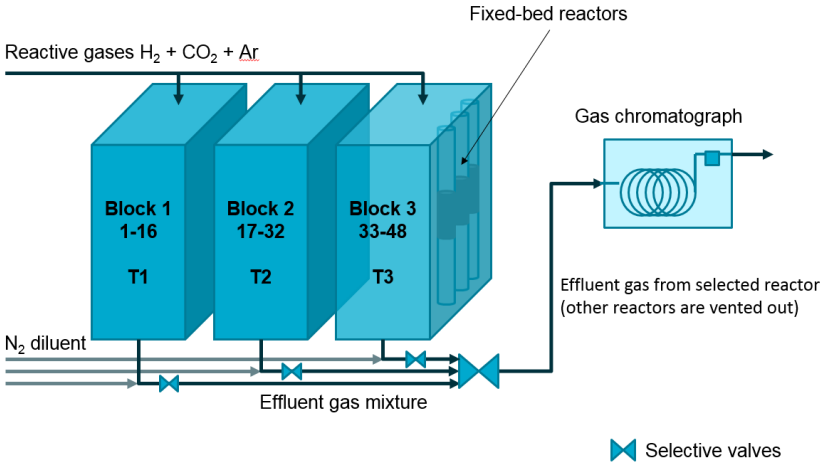

Figure S2: Diagram of the multi-channel rig used for the catalysis testing.

Experimental conditions

In a typical catalysis test, approximately 20 mg of precatalyst or catalyst mixed with 50 mg of SiC were loaded over a SiC bed inside a steel or quartz micro reactor and placed in the rig. The samples were then heated at 2 °C/min under a N_2 stream (3 mL/min) to 220 °C at 1 bar and kept for 20 min in order to remove guest solvent molecules from the samples. Next the samples were exposed to the reactive gas mixture and to set conditions of temperature (ramp rate of 5 °C/min) and pressure (4 bar/min) while the test was carried continuously for several hours. The reactive gas mixture had 3% argon and 97% CO_2 and H_2 either in a stoichiometric ratio (1 CO_2 : 4 H_2) or with H_2 as the limiting reactant (1 CO_2 : 3.5 H_2). Gas effluent composition was finally analyzed by a gas chromatograph (GC) as described above. It is important to mention that the CO_2 methanation is a volume reducing reaction, meaning that increasing pressure may improve the conversion of CO_2.[7] However, due to technical restrictions our studies were performed at 5 bar and above, for validation and comparison purposes the commercial catalyst Methanizer was included in the experiments.

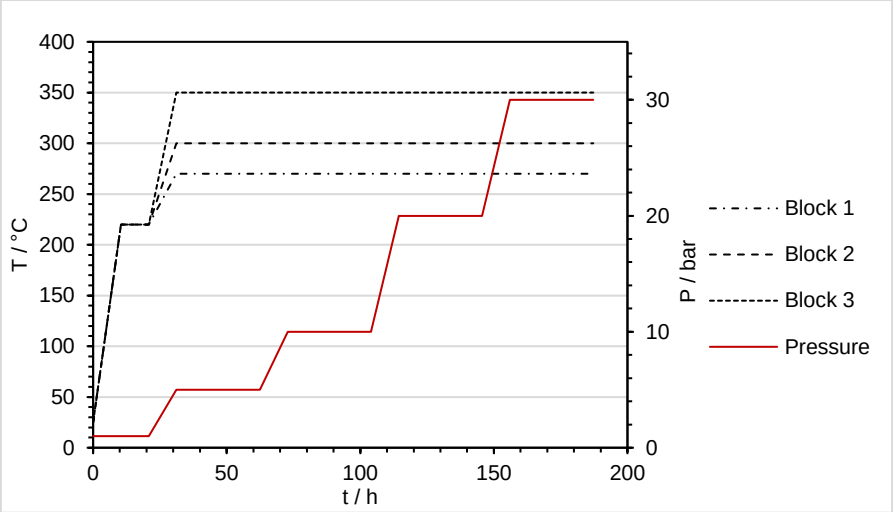

Figure S3: Experimental conditions versus time for the catalytic performance comparison of different supports (**Figure 3**). The first step at 1 bar and up to 220 °C was carried under N_2 and lasts for 20 min, it has been stretched in this plot for the purpose of observation.

Catalysis data analysis

Weight hourly space velocity (WHSV)

Weight hourly space velocity (WHSV) is defined as the volume of gas fed to each reactor per gram of final catalyst loaded per hour. Mass of final catalyst was defined as 35% of the precatalyst according to the mass loss measurements and to TGA.

$$WHSV\ (L \cdot h^{-1} \cdot g^{-1}) = \frac{\dot{V}_{gas\ fed\ in\ reactor}}{M_{final\ catalyst}} = \frac{\dot{V}_{H_2} + \dot{V}_{CO_2} + \dot{V}_{Ar}}{M_{pre-catalyst} * 0.35}$$

Quantitative analysis of reactor effluent gas via GC

For the quantitative analysis, the gas chromatograph (GC) was calibrated by flowing a gas mixture with known amounts of ethane, ethene, acetylene, methane, carbon dioxide, carbon monoxide, hydrogen and argon, supplied by Coregas, diluted with N_2 stream at different dilution ratios to define the factor$_i$ (area/%) used in the analysis and OpenLab software from Agilent was used to define species retention time.

$$x_{i\ effluent} = \frac{GC\ Area_i}{factor_i}$$

Conversion and selectivity calculations

Ar was added to the reactor gas feed as tracer gas. Since N_2 by-pass the reactor in order to dilute the gas effluent, just as Ar it does not react and thus its fraction in the gas effluent can be directly correlated with a total volume flow change. Both N_2 and Ar were used for verification.

$$\dot{V}_{reactor\ gas\ feed} = \dot{V}_{H_2 feed} + \dot{V}_{CO_2 feed} + \dot{V}_{Ar\ feed}$$

$$\dot{V}_{total\ feed} = \dot{V}_{reactor\ gas\ feed} + \dot{V}_{by-pass\ N_2 feed}$$

$$\dot{V}_{total\ effluent} = \dot{V}_{H_2 effluent} + \dot{V}_{CO_2 effluent} + \dot{V}_{Ar\ effluent} + \dot{V}_{N_2 effluent} + \sum_i \dot{V}_{product_i}$$

$$\dot{V}_{N_2 fed} = \dot{V}_{N_2 effluent} = \dot{V}_{total\ effluent} \cdot x_{N_2\ effluent} \leftrightarrow \dot{V}_{total\ effluent} = \frac{\dot{V}_{N_2 fed}}{x_{N_2\ effluent}}$$

$$\dot{V}_{Ar\ fed} = \dot{V}_{Ar\ effluent} = \dot{V}_{total\ effluent} \cdot x_{Ar\ effluent} \leftrightarrow \dot{V}_{total\ effluent} = \frac{\dot{V}_{Ar fed}}{x_{Ar\ effluent}}$$

Species effluent volume flow

$$\dot{V}_{i\ effluent} = \dot{V}_{total\ effluent} \cdot x_{i\ effluent}$$

H_2 conversion values for single data points

$$X_{H_2} = \frac{\dot{V}_{H_2\ consumed}}{\dot{V}_{H_2\ fed}} = \frac{\dot{V}_{H_2\ fed} - \dot{V}_{H_2\ effluent}}{\dot{V}_{H_2\ fed}}$$

Reported multiple data points average H_2 conversion values

$$X_{H_2} = \frac{\sum \dot{V}_{H_2\ consumed}}{\sum \dot{V}_{H_2\ fed}} = \frac{\sum \dot{V}_{H_2\ fed} - \sum \dot{V}_{H_2\ effluent}}{\sum \dot{V}_{H_2\ fed}}$$

Reported average conversions were calculated for periods after catalyst activation, which varied from 4 up to 13 hours depending on the temperature.

Standard deviation for H_2 conversion presented in this work was calculated by the analysis of H_2 conversion values for single data points.

Selectivity was also confirmed by the absence of other products as observed in **Figure S4**.

$$S_{CH_4} = \frac{\dot{V}_{CH_4\ effluent}}{\dot{V}_{CO_2\ consumed}}$$

$$S_{CO} = \frac{\dot{V}_{CO\ effluent}}{\dot{V}_{CO_2\ consumed}}$$

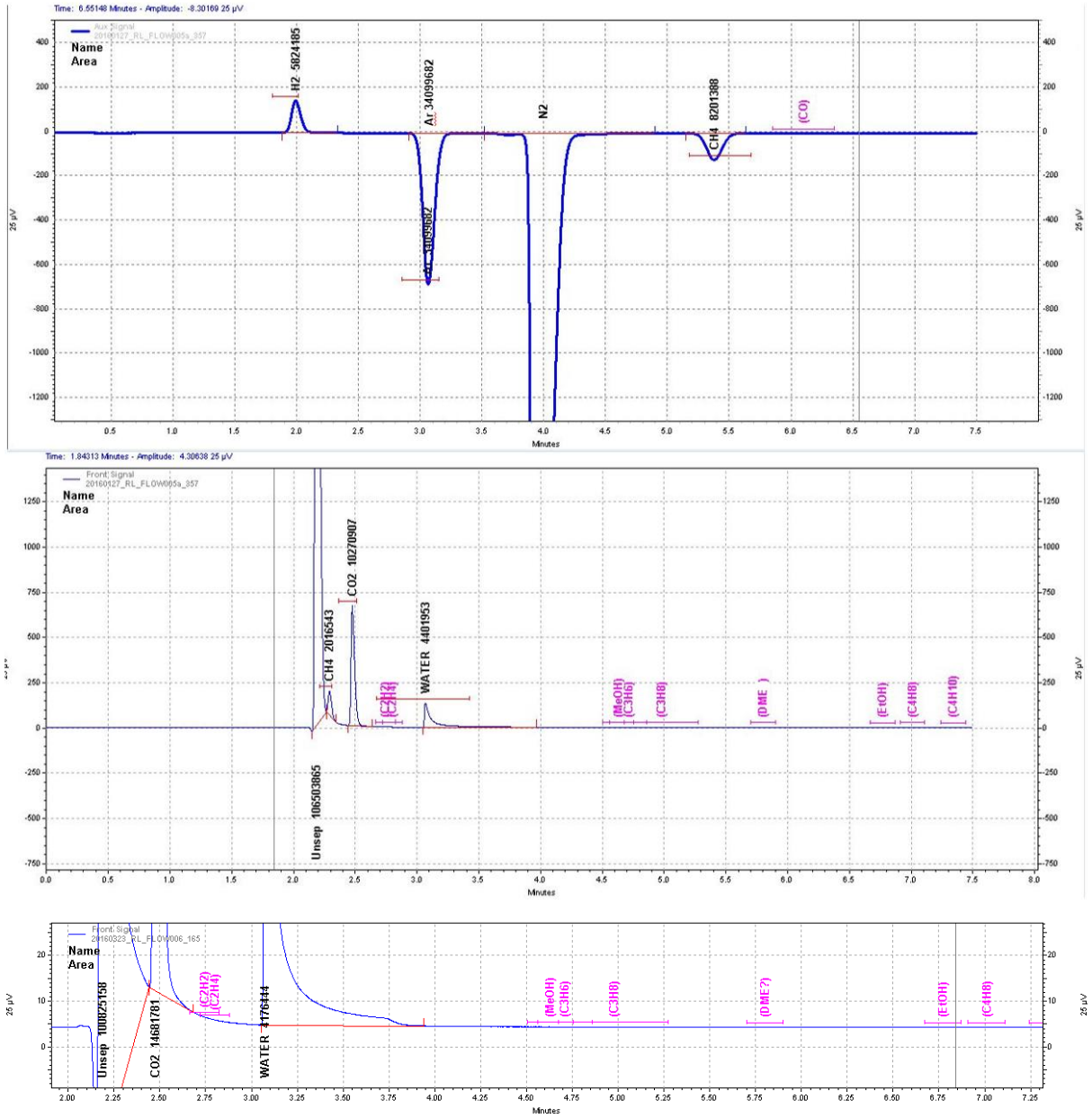

Figure S4: Example of the gas chromatograms obtained for each of the channels during the catalysis testing. The auxiliary channel (top) was used for H_2 and methane quantification and the front channel (middle) was used for CO_2 quantification and to verification of other products formation. CH_4 quantification was used to verify H_2 conversion numbers, as CO_2 could only be estimated as its peak position, on the tail of the unseparated gases peak, limited the accuracy of its quantification (bottom). This method was chosen because identification of small quantities of high molecular weight species was desired and we calibrated and trust the dosage of CO_2 to the reactor as discussed below.

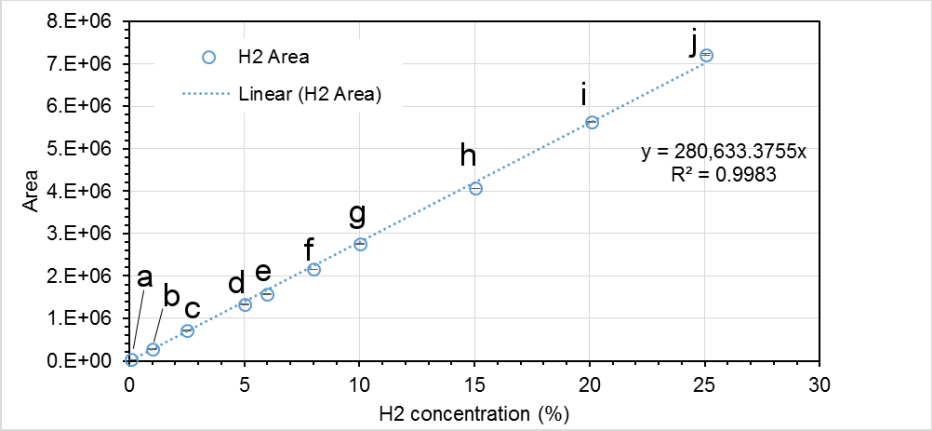

Figure S5: The H_2 calibration curve for the gas chromatograph and method used for this work. The peak shape at each concentration is displayed in **Figure S6**. Each point indicates the average of 3 to 4 injections for the same concentration. Error bars, present inside the markers, indicate standard deviation of the area.

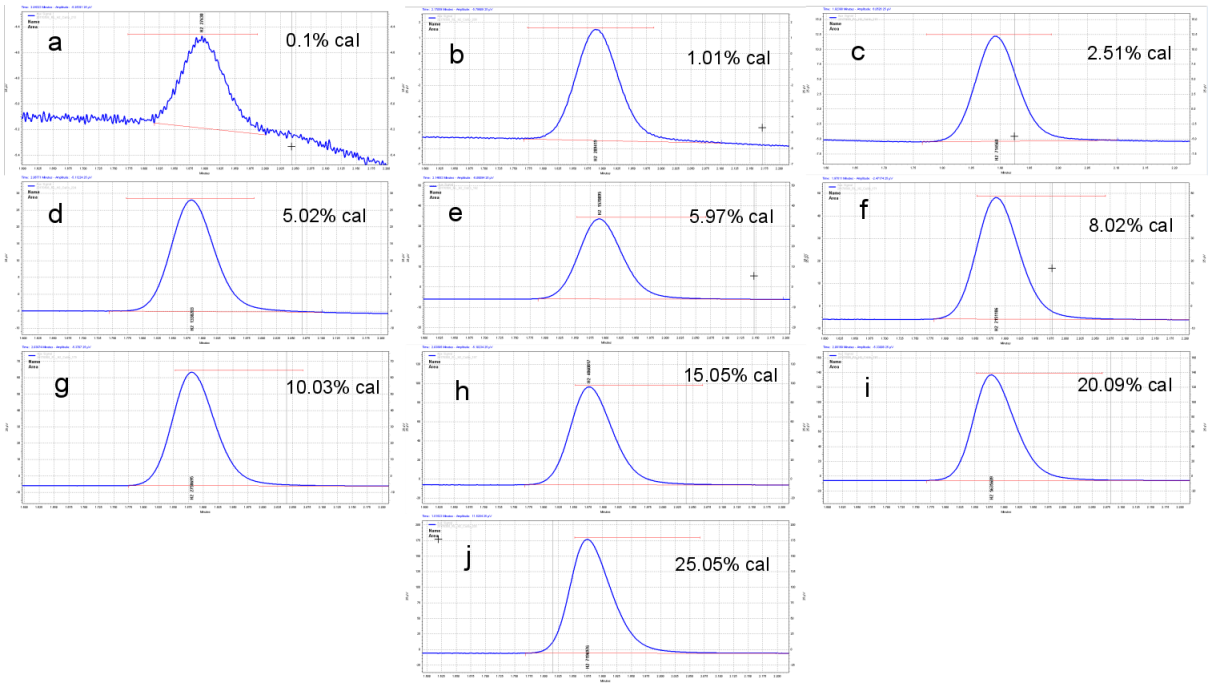

Figure S6: H_2 chromatogram peaks during calibration with different concentrations of H_2 as indicated in the figure.

Mass balance

Carbon balance was done by considering CH_4 production, CO_2 composition in the gas feed, absence of any other C-containing product and carbon content in catalyst. The CO_2 feed is accurately measured and according to the carbon mass balance method described below, the methane Yield (Y_{CH4}) is approximately equal to the CO_2 delivered to the reactor.

Gas feed composition (input) was controlled using EL-Flow Bronkhorst mass flow controllers calibrated by Bronkhorst. Spot checks are regularly done to verify the flow through each reactor. GC analysis of empty reactors are also performed to check the mass flow controllers' accuracy. In all experiments, empty reactors were added to the experiment and tested in parallel to verify the gas composition in the absence of catalysts. Composition of gas effluent was analysed using a GC.

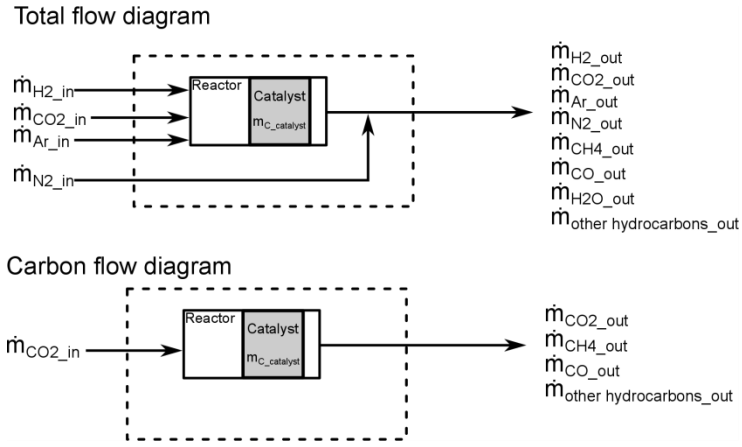

Figure S7: Flow diagram for all molecules (top) and for carbon-containing molecules only (bottom).

Below the mass balance for carbon-containing molecules.

$$input - output - accumulation = 0$$

Here, accumulation is defined as carbon deposited on the catalyst.

$$\dot{m}_{CO_{2_{in}}} - \dot{m}_{CO_{2_{out}}} - \dot{m}_{CH_{4_{out}}} - \dot{m}_{CO_{out}} - \dot{m}_{other\ hydrocarbons_{out}} - \dot{m}_{C_{catalyst}} = 0$$

- No other hydrocarbons were observed in the GC **Figure S4**, therefore

  $\dot{m}_{other\ hydrocarbons_{out}} = 0$

- After activation of the catalyst there is no carbon left in the sample (**Figure S11**)

  $\dot{m}_{C_{catalyst}} \cong 0$

- Selectivity of CO is less than 0.2% (**Figure 2D**)

  $\dot{m}_{CO_{out}} \cong 0$

$$\dot{m}_{CO_{2_{in}}} - \dot{m}_{CO_{2_{out}}} - \dot{m}_{CH_{4_{out}}} \cong 0$$

$$\dot{m}_{CO_{2_{in}}} - \dot{m}_{CO_{2_{out}}} \cong \dot{m}_{CH_{4_{out}}} \xRightarrow{\div\left(\dot{m}_{CO_{2_{in}}}\right)} \frac{\dot{m}_{CO_{2_{in}}} - \dot{m}_{CO_{2_{out}}}}{\dot{m}_{CO_{2_{in}}}} \cong \frac{\dot{m}_{CH_{4_{out}}}}{\dot{m}_{CO_{2_{in}}}}$$

$$\frac{\dot{m}_{CO_{2_{in}}} - \dot{m}_{CO_{2_{out}}}}{\dot{m}_{CO_{2_{in}}}} = X_{CO_2} \cong Y_{CH_4} = \frac{\dot{m}_{CH_{4_{out}}}}{\dot{m}_{CO_{2_{in}}}}$$

At stoichiometric ration H_2:CO_2 = 4:1, it is possible to compare the methane yield to the H_2 conversion for validation of the results.

$$\frac{\dot{m}_{CO_{2_{in}}} - \dot{m}_{CO_{2_{out}}}}{\dot{m}_{CO_{2_{in}}}} = X_{CO_2} \cong Y_{CH_4} = \frac{\dot{m}_{CH_{4_{out}}}}{\dot{m}_{CO_{2_{in}}}} = \frac{\dot{m}_{H_{2_{in}}} - \dot{m}_{H_{2_{out}}}}{\dot{m}_{H_{2_{in}}}} = X_{H_2}$$

This comparison is presented in **Figure S8**.

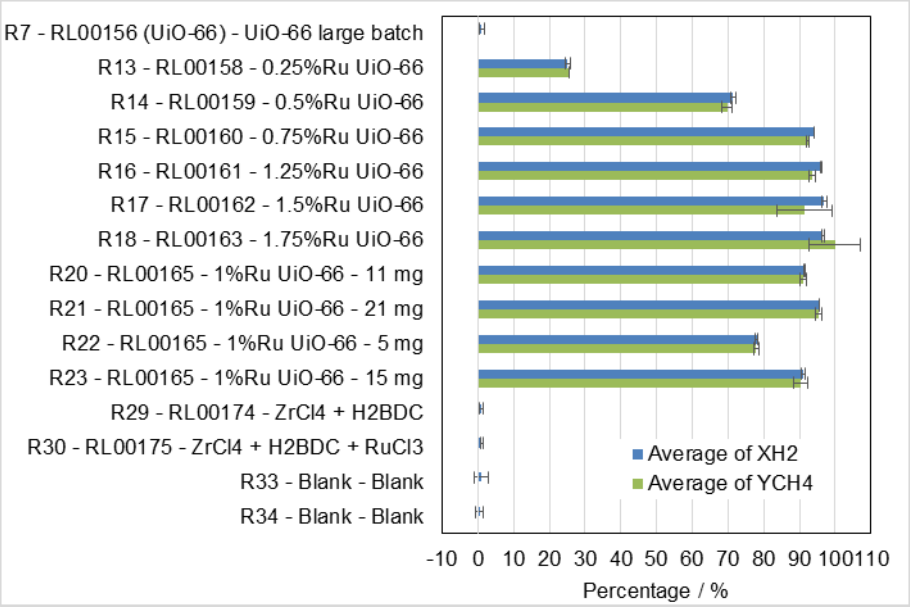

Figure S8: Example of verification of H_2 conversion ($ml\_H_{2\ consumed}/ml\_H_{2\ in}$) and CH_4 yield ($ml\_CH_{4\ produced}/ml\_CO_{2\ in}$) for different samples tested in parallel.

Transmission electron microscopy (TEM)

Figure 6A, 6B and S18: Samples were prepared for TEM as follows: aliquots of sample were suspended in ethanol, and applied to carbon-coated copper TEM grids. After air drying, grids were examined in a Tecnai 12 G2 TEM (FEI, The Netherlands), operating at 120 kV, and images were recorded with a MegaView III CCD (Olympus, Tokyo).

Figure 6C and 6D: High Resolution TEM was performed in a Tecnai F20 TEM (FEI, The Netherlands) equipped with STEM and EDS detectors operating at 200 kV.

Figure 8 and S21: TEM/STEM investigation was performed using a probe-corrected JEOL ARM200F (JEOL, USA) equipped with a cold field emission gun operating at 200 kV. High-angle annular dark-field (HAADF) images were acquired with inner and outer collection angles of 68 and 280 mrad, respectively, while bright field images were acquired with a maximum collection angle of 17 mrad. All images were acquired with a 20 ms dwell time and convergence angle of 25 mrad, resulting in a probe size about 0.1 nm and a current of 40 pA. The Energy-dispersive X-ray Spectroscopy (EDS) maps were acquired with a probe current of 155 uA.

Scanning electron microscopy (SEM/EDS)

Figure 7 and S19: The samples, which were mounted on TEM grids as described above, were placed on a STEM stage so that the samples could be imaged using a Zeiss Merlin FESEM (Field Emission Scanning Electron Microscope) operated in the secondary electron (SE) mode and back-scattered mode (BSE). SE images highlight topographical features whereas BSE imaging enhances elemental contrast and oxidation state differences so that low atomic elements or oxidated elements appear darker and higher atomic number elements or in the elemental state appear brighter. Energy dispersive spectroscopy (EDS) was used to identify elements present within the samples. The EDS system used was AZTEC, manufactured by Oxford Instruments Pty Ltd. An accelerating voltage of 25 kV was used for EDS mapping. The magnifications used are indicative of the scale bars shown in the images.

X-ray photoelectron spectroscopy (XPS)

X-ray photoelectron spectroscopy (XPS) analysis was performed using an AXIS Ultra DLD spectrometer (Kratos Analytical Inc., Manchester, UK) with a monochromated Al K_α source at a power of 180 W (15 kV × 12 mA), a hemispherical analyser operating in the fixed analyser transmission mode and the standard aperture (analysis area: 0.3 mm × 0.7 mm) The total pressure in the main vacuum chamber during analysis was typically 10^{-8} mbar. Survey spectra were acquired at a pass energy of 160 eV. To obtain more detailed information about chemical structure, oxidation states etc., high resolution spectra were recorded from individual peaks at 40 eV pass energy (yielding a typical peak width for polymers of 0.9 – 1.0 eV).

The sample was filled into a shallow well of a custom-built sample holder where the sample was analysed at two different locations at a nominal photoelectron emission angle of 0º w.r.t. the surface normal. Since the actual emission angle is ill-defined in the case of particles (ranging from 0º to 90º) the sampling depth may range from 0 nm to approx. 10 nm. In the case of a rough surface, such as the sample analyzed, the angle of emission vary greatly across the surface, making this technique more surface sensitive.

XPS Quantitative analysis

Data processing was performed using CasaXPS processing software version 2.3.15 (Casa Software Ltd., Teignmouth, UK). All elements present were identified from survey spectra. The atomic concentrations of the detected elements were calculated using integral peak intensities and the sensitivity factors supplied by the manufacturer. Correction of the binding energy scale for sample charging was based on the main C 1s peak, located at either 284.5 eV (sp2 hybridized carbon in C60) or 285 eV (aliphatic hydrocarbon). The accuracy associated with quantitative XPS is ca. 10% - 15%.

Si, Na and C shown in the analysis are sample contaminants.

Satellite peaks were observed on the high binding energy side of the Zr 3d peaks, as demonstrated in **Figure S22** and **S23**. A number of factors can contribute to the overall spectral shape. In terms of intrinsic contributions, in addition to an asymmetric tail on the higher binding energy side of the peak, spectral contributions from plasmons can occur as a result of coupling of core hole with collective electron oscillations for free-electron like metals[8] or shake-up peaks originating from π-π*transitions in aromatic and unsaturated species such as polystyrene.[9] Similar spectral shapes as observed herein at binding energies greater than the main Zr 3d doublet have been observed for polycrystalline pure[10] and oxidised[11] zirconium. In the case of ZrO_2-based ceramics,[12] a loss structure comprising of three peaks has been observed, which are assigned to excitation of ligand electrons in the valence band to the conduction band, bulk plasmon and excitation of a Zr core level, respectively. The binding energy shift from the main peak for the first two peaks matches that observed for **Figure S23**, noting that the binding energy ranged selected was not sufficient to collect the spectral region expected for the third peak. Considering the binding energy positions of the peaks, the overall spectral shape and the structure of the ligand-based MOF explored herein, the assignments obtained from ZrO_2-based ceramic are likely the closest representation for the loss structure observed herein for the Zr 3d peak.. The ratio of the Ru 3d and C 1s contributions to the total peak area of this spectral region were determined via fitting of the high resolution spectra using the protocol detailed by Morgan.[13] The ratio of intensity of the total Ru 3d and C 1s contributions was used to scale the total peak area of the Ru 3d / C 1s region defined in the survey spectra and thus calculate the elemental quantification of the catalyst. Satellite peaks were also assigned to the fitting of the Ru 3d and C 1s spectra, where Morgan attributed these to plasmons.[13]

DFT Simulations

The UiO-66 configurations were optimized by density functional theory (DFT) calculations performed using the SIESTA code[14] with the generalized gradient approximation of Perdew-Burke-Ernzerhof (PBE).[15] Norm-conserving Troullier-Martins pseudopotentials with scalar relativistic correction were used. The wave functions were expanded in a double-ζ polarized basis set (DζP). A 200 Ry cutoff for the density integration grid and a density matrix convergence criterion of $2x10^{-4}$ were chosen. A simple cubic superlattice with a cell size of 30 Å was used. In order to determine the most stable configuration, all atoms were allowed to relax until the Hellmann–Feynman forces were smaller than 5 meV.$Å^{-1}$ by using the conjugate gradient minimization method. These combinations of parameters have been successfully proven in different DFT studies.[16, 17]

The atomic models were constructed from periodic unit cells of the catalyst precursor UiO-66. In each configuration the Ru atom is placed in different sites (**Figure 9**) with bond lengths of 2.1 Å and 3.4 Å between ruthenium and oxygen atoms and ruthenium and zirconium atoms respectively. Each configuration was relaxed prior to the geometry optimization.

Supporting results

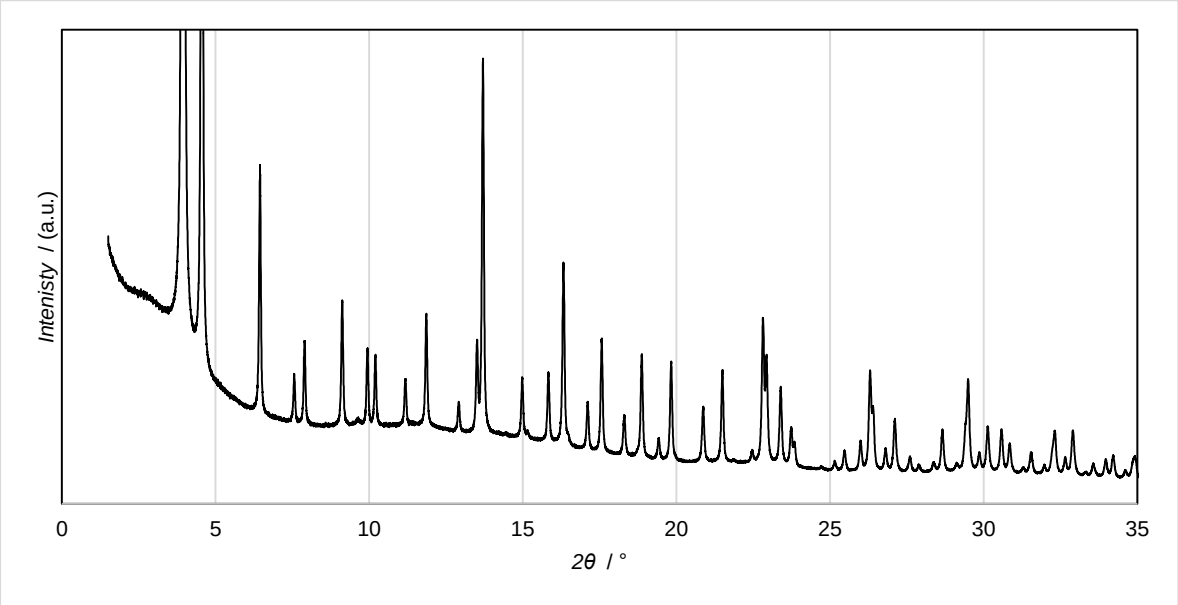

Figure S9: Synchrotron source (15 keV) X-ray diffractogram of Ru-impregnated UiO-66 (**1Ru/UiO-66**) pre-reduced in a tube furnace at 250 °C and 1 bar in 5% H_2-N_2 for 4 h. The UiO-66 structure persisted after the heat treatment and no Ru^0, RuO_2 or $RuCl_3$ phase is observed. **Figure S19** shows the presence of Cl in this sample, we believe the chlorine atoms are well dispersed within the framework due to the absence of chlorides reflections.

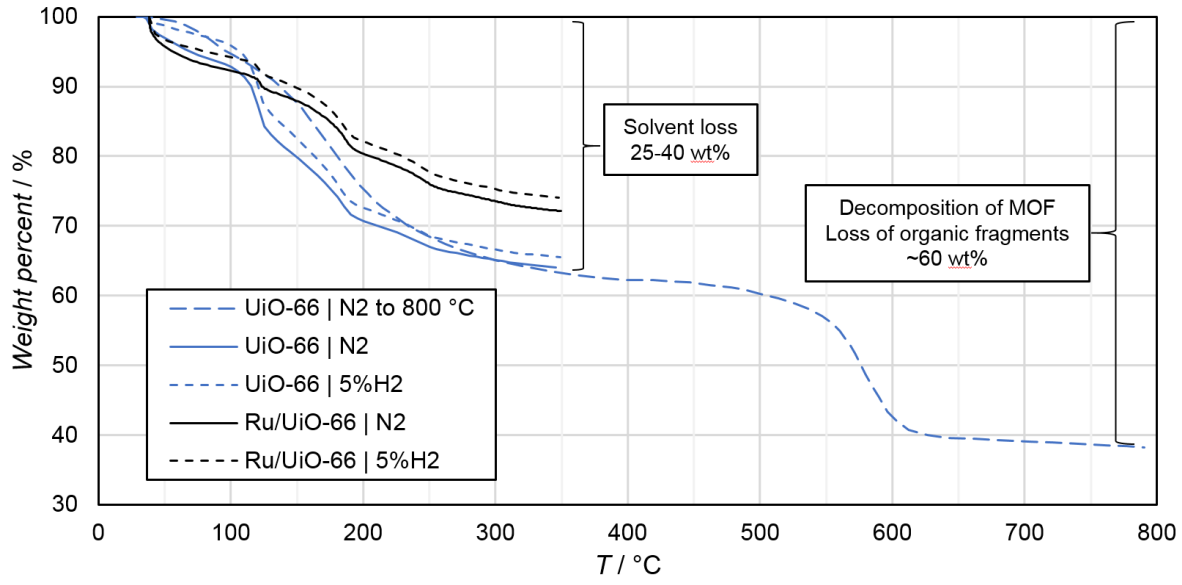

Figure S10: TGA thermograms of UiO-66 (blue) and **1Ru/UiO-66** (Black) in different purge gases (N_2 and 5%H_2/N_2). The presence of 5% H_2 did not seem to affect the stability of the MOF under 350 °C. In pure N_2, the decomposition of the framework (24 % mass loss) occurs after 400 °C. Since the weight loss differs minimally among these samples, we could conclude that a low concentration of H_2 (5 v%) was not enough for the decomposition of UiO-66 or **1Ru/UiO-66** below 350 °C.

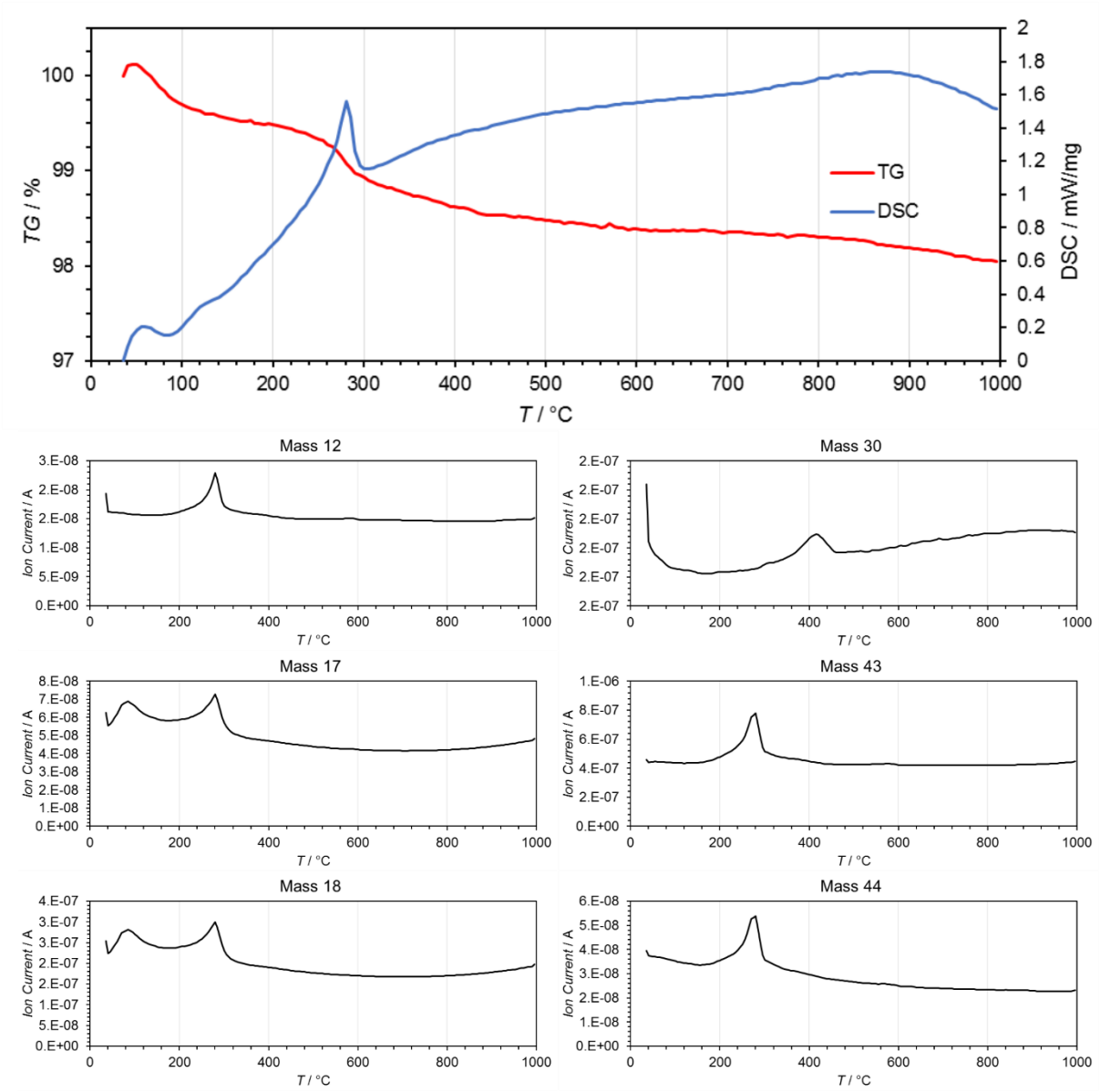

Figure S11: Simultaneous Thermal Analysis (STA) and Evolved Gas Analysis (EGA) of used MOF-derived catalyst performed in air. The TGA results shows less than 2% mass loss during the analysis, EGA confirmed the loss of carbon/carbon containing species (m=12, 30, 43 and 44) and H_2O (m=17 and 18). Thus, this is further evidence that no carbon is left in the catalyst after the *in situ* activation and the present carbon is adventitious. Sample: activated MOF-derived Ru-ZrO_2 catalyst after use at 350 °C, H_2:CO_2 = 4:1.

Table S3: Mass loss of **1Ru/UiO-66** during the catalyst activation. Weight of reactors were measured before precatalyst loading, after precatalyst catalyst loading and after catalysis test. The values below are difference between the loaded reactor weight, before and after catalysis. The mass loss around 60% can be related to the MOF decomposition (**Figure S12**).

Activation temp (°C)	Precatalyst **1Ru/UiO-66** (g)	MOF-derived catalyst (g)	Mass loss (wt%)
250	0.0534	0.0191	64
250	0.0504	0.0178	65
300	0.0487	0.0198	59
300	0.0475	0.0181	62
350	0.0454	0.0198	56
350	0.0462	0.0155	66

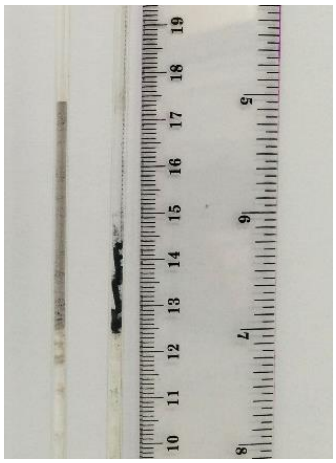

Figure S12: Photograph of **1Ru/UiO-66** as synthesized loaded in a micro-reactor (left) and of the activated MOF-derived Ru-ZrO_2 catalyst after use at 350 °C and 30 bar for 20 hours, H_2 : CO_2 = 4 : 1, WHSV = 25 $L \cdot h^{-1} \cdot g^{-1}$ (right). Ruler units are cm (left) and inches (right).

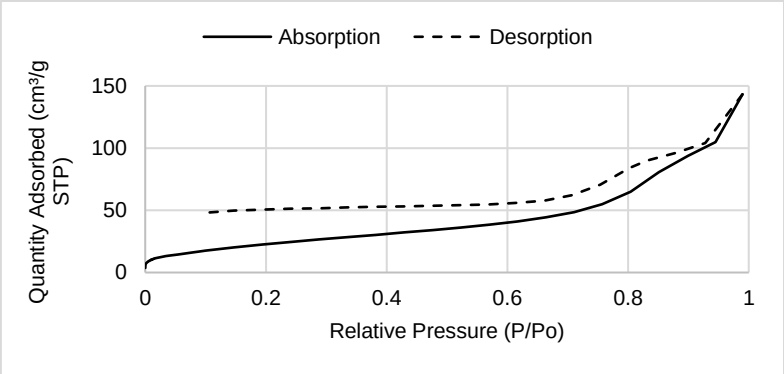

Figure S13: N_2 absorption isotherm at 77K for MOF-derived Ru-ZrO_2 catalyst after use. BET Surface area was found to be 60 m^2/g. Reaction conditions: 350 °C, 30 bar, H_2:CO_2 = 4:1, WHSV = 8.7 L·h-1·precatalyst g^{-1}.

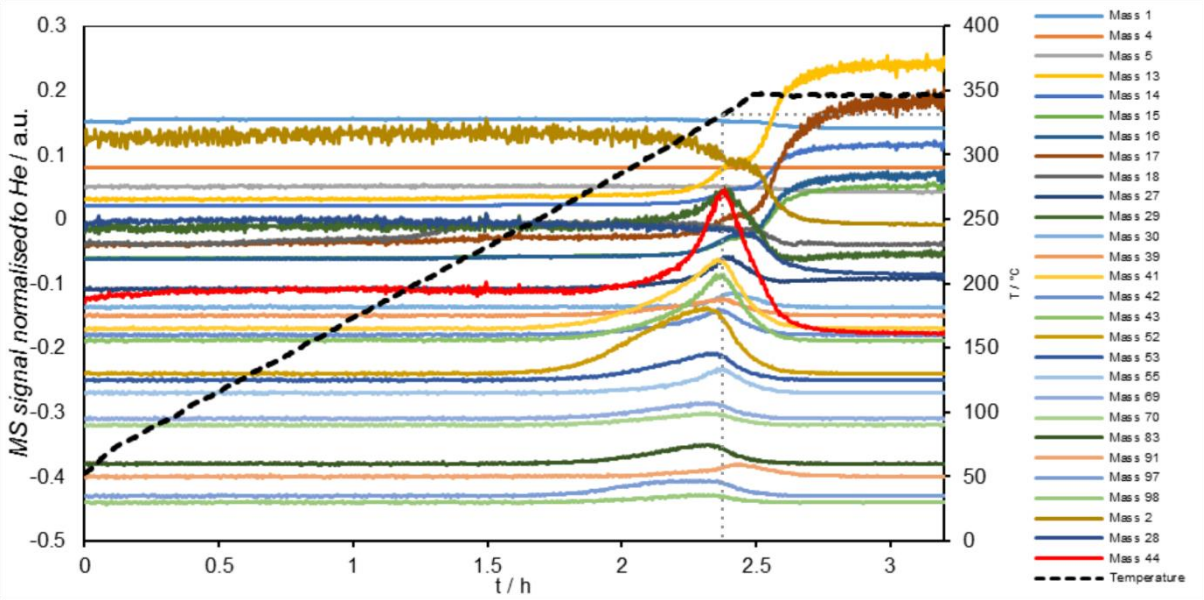

Figure S14: Mass spectral signal normalized to He tracing monitoring the activation of the MOF-derived catalyst. Several different organic fragments are detected by the mass spectrometer at 330 °C (dashed black line). Total experiment time: 3 h. Reaction conditions: 60 mg of **1Ru/UiO-66**, H_2:CO_2 = 3:1 (63.75% H_2, 21.25% CO_2 and 15% He), WHSV = 200 $L \cdot h^{-1} \cdot g_{cat}^{-1}$. Data was scaled and offset along the y axis for clarity.

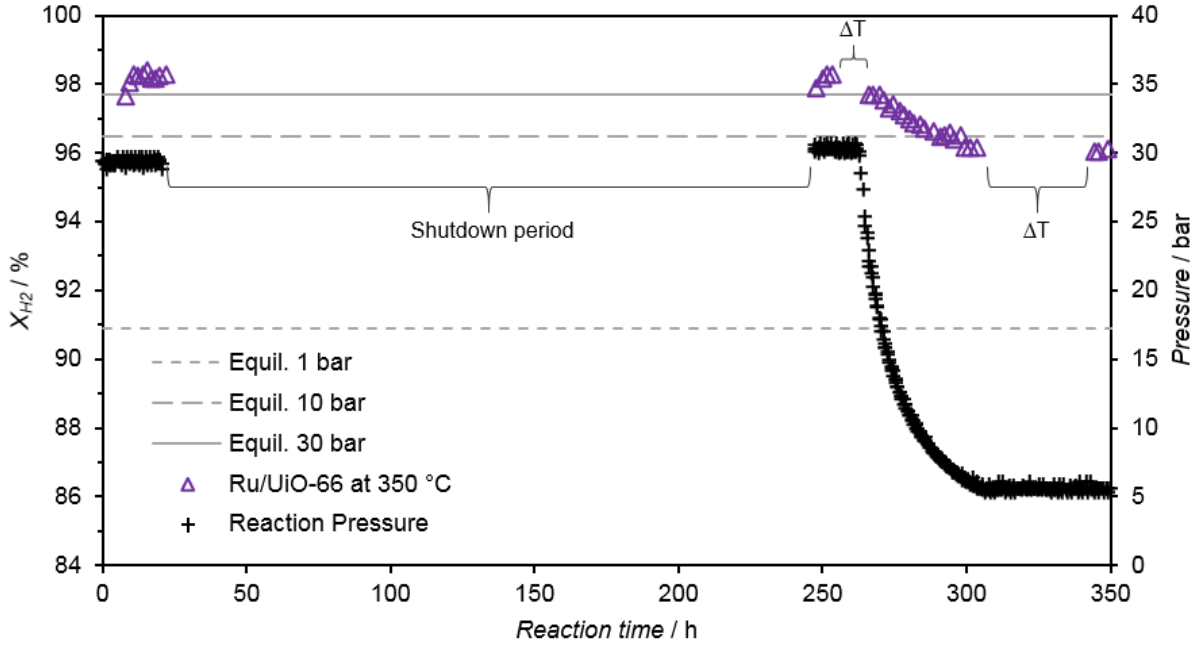

Figure S15: Triangle markers indicate the X_{H2} for the Ru-UiO-66 derived catalyst at 350 °C. Initially, the catalyst was tested at 30 bar before a long shutdown period, where the samples were cooled down to room temperature and exposed to air at atmospheric pressure. The sample was then tested again at 30 bar without any sign of deactivation. Next, it was tested at decreasing reaction pressure conditions to 5 bar (cross markers). The following periods where X_{H2} is absent are periods where the sample was tested at different temperatures (Figure 1B). For comparison, the gray lines indicate the X_{H2} calculated for the thermodynamic equilibrium at 350 °C and different pressures for CO_2 methanation with equal H_2 to CO_2 ratio[7]. Reaction conditions: 50 mg of **1Ru/UiO-66**, H_2:CO_2 = 4:1, WHSV = 43 $L \cdot h^{-1} \cdot g^{-1}$.

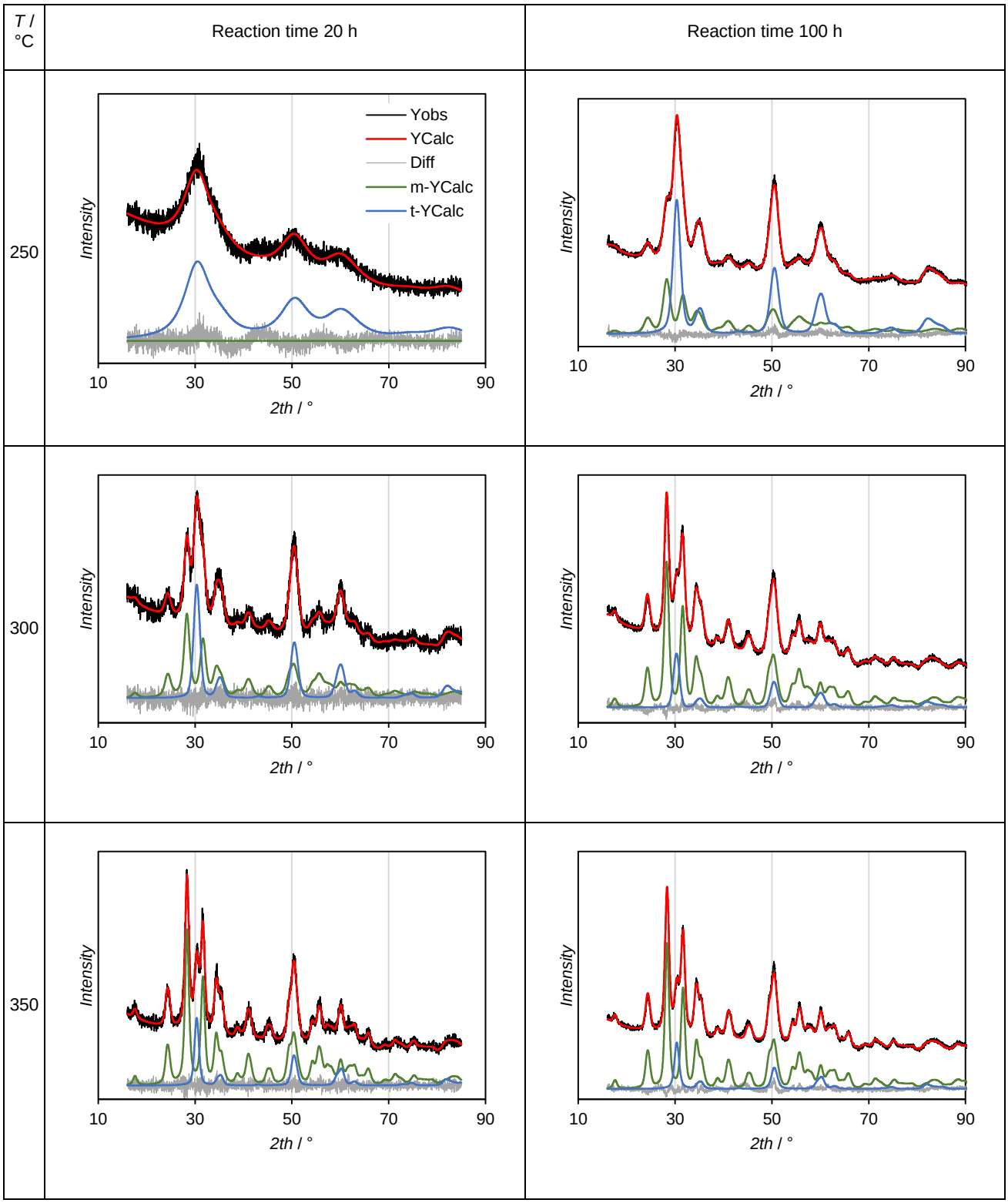

Figure S16: Analysis of PXRD data of the MOF-derived catalysts activated at different temperatures at during different reaction times. Observed XRD (Yobs), calculated XRD pattern through Rietveld method (Ycalc), difference curve (Diff), calculated contribution for the ZrO_2 monoclinic phase (m-Ycalc) and for the ZrO_2 tetragonal phase (t-Ycalc). No other phase (graphite, RuO_2 or Ru^0) was observed. Reaction conditions: 50 mg of **1Ru/UiO-66**, H_2:CO_2 = 4:1, WHSV = 43 $L \cdot h^{-1} \cdot g^{-1}$ and 30 bar. Refined parameters and the weighted profile R factor (r_wp) can be found in **Table S4**.

Table S4: Rietveld refinement results according to reaction conditions.

Sample	Activation temp (°C)	Activation pressure (bar)	Reaction time (h)	Phase	Amount of phase (Wt%)	error	Rietveld Scale Factor	a (nm)	b (nm)	c (nm)	β (°)	r_wp	lvol - Crystallite domain size (nm)	error	e0 - micro strain	error
1	250	30	20	t-ZrO2	100	0.00	0.005789	3.589	3.589	5.225	90	5.80	1.84	0.00	0.02051	0.00
2	300	30	20	m-ZrO2	61.59	1.06	0.000623	5.156	5.202	5.329	99.38	5.48	8.32	0.72	0.00011	306.32
2	300	30	20	t-ZrO2	38.41	1.06	0.001628	3.602	3.602	5.185	90	5.48	7.73	0.59	0.00009	417.35
3	350	30	20	m-ZrO2	82.57	0.46	0.001486	5.151	5.208	5.322	99.22	4.85	12.09	0.47	0.00004	215.73
3	350	30	20	t-ZrO2	17.43	0.46	0.001312	3.600	3.600	5.197	90	4.85	10.92	1.03	0.01553	1.88
4	250	30	100	m-ZrO2	45.55	0.47	0.004795	5.160	5.194	5.323	99.43	2.32	6.68	0.25	0.00012	227.63
4	250	30	100	t-ZrO2	54.45	0.47	0.024072	3.595	3.595	5.185	90	2.32	6.49	0.12	0.00018	62.65
5	300	30	100	m-ZrO2	83.48	0.40	0.006676	5.154	5.206	5.321	99.30	2.98	10.47	0.20	0.00009	51.07
5	300	30	100	t-ZrO2	16.52	0.40	0.005531	3.597	3.597	5.201	90	2.98	8.23	0.48	0.01018	1.54
6	350	30	100	m-ZrO2	84.83	0.28	0.008906	5.151	5.207	5.318	99.24	2.87	11.88	0.21	0.00012	33.82
6	350	30	100	t-ZrO2	15.17	0.28	0.00667	3.600	3.600	5.191	90	2.87	10.14	0.60	0.0002	72.41

T / °C	20 h			100 h		
	m-ZrO_2	t-ZrO_2	X_{H2} / %	m-ZrO_2	t-ZrO_2	X_{H2} / %
250	0	100	23	48	52	28
300	52	48	22	86	14	53
350	82	18	96	88	12	96

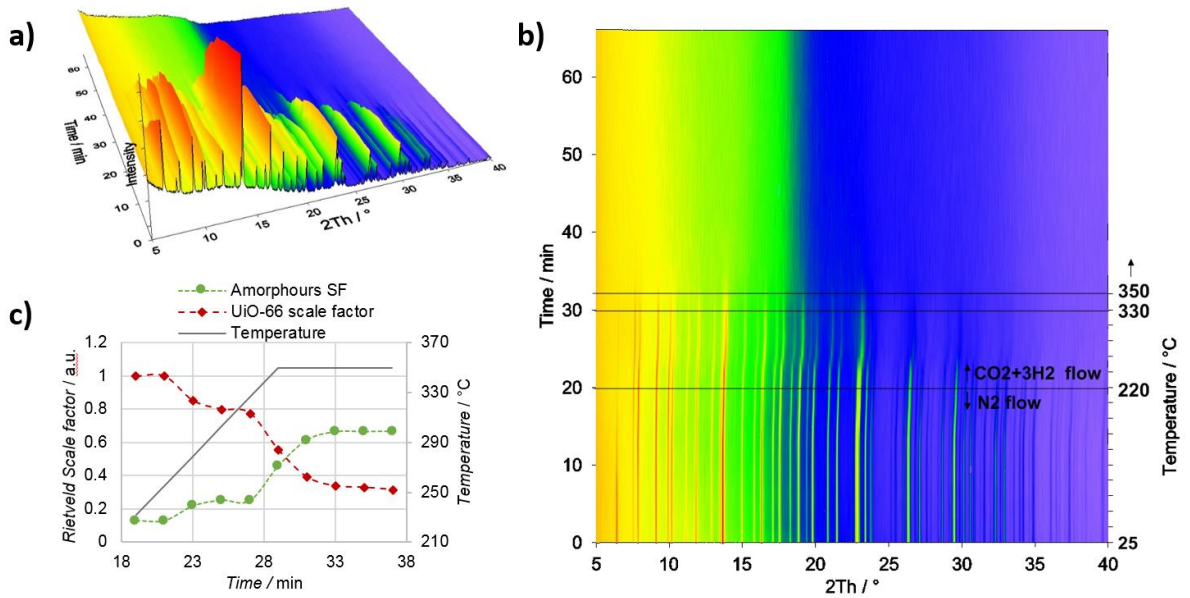

Figure S17: a, b) *In situ* variable temperature PXRD of **1Ru/UiO-66**. The sample was first heated to 220 °C under N_2 flow, then at 19 min, the gas flow was replaced with a mixture of CO_2:H_2 = 1:3. Upon reaching 350 °C, the temperature was kept constant. c) Rietveld refinement scale factor versus time and temperature for UiO-66 crystalline phase[18] and the resulting amorphous phase. Rietveld scale factor is a multiplier of the reflections of a certain phase (relative intensities within a phase are constant) and it can be correlated to the relative amount of the phase in the sample. A drastic decrease of the UiO-66 scale factor was observed simultaneously with the increase of the amorphous phase contribution. The Rietveld refinement of this XRD dataset was performed in batch mode starting with the diffractogram at 19min. The values refined for each diffractogram were used as input for the next. The background contribution for all diffractograms was fixed according to the refined values at 19min.

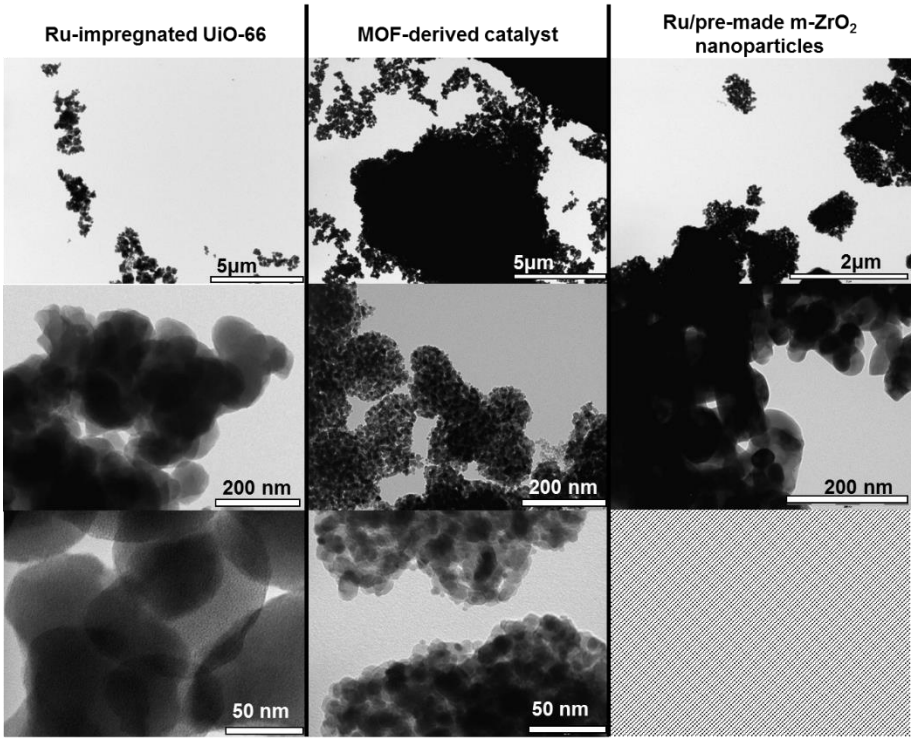

Figure S18: TEM images of **1Ru/UiO-66** pre-reduced in a tube furnace at 250 °C in 5% H_2-N_2 for 4 hours, UiO-66 framework was retained and confirmed by XRD (**Figure S9**) (left); MOF-derived catalyst activated at 350 °C and 30 bar (centre); and Ru/pmZrO2, Ru on premade m-ZrO_2, tested at 350 °C and 30 bar (right). The MOF-derived sample is composed of ZrO_2 nanoparticles, organized in clusters which resemble the UiO-66 crystals shape.

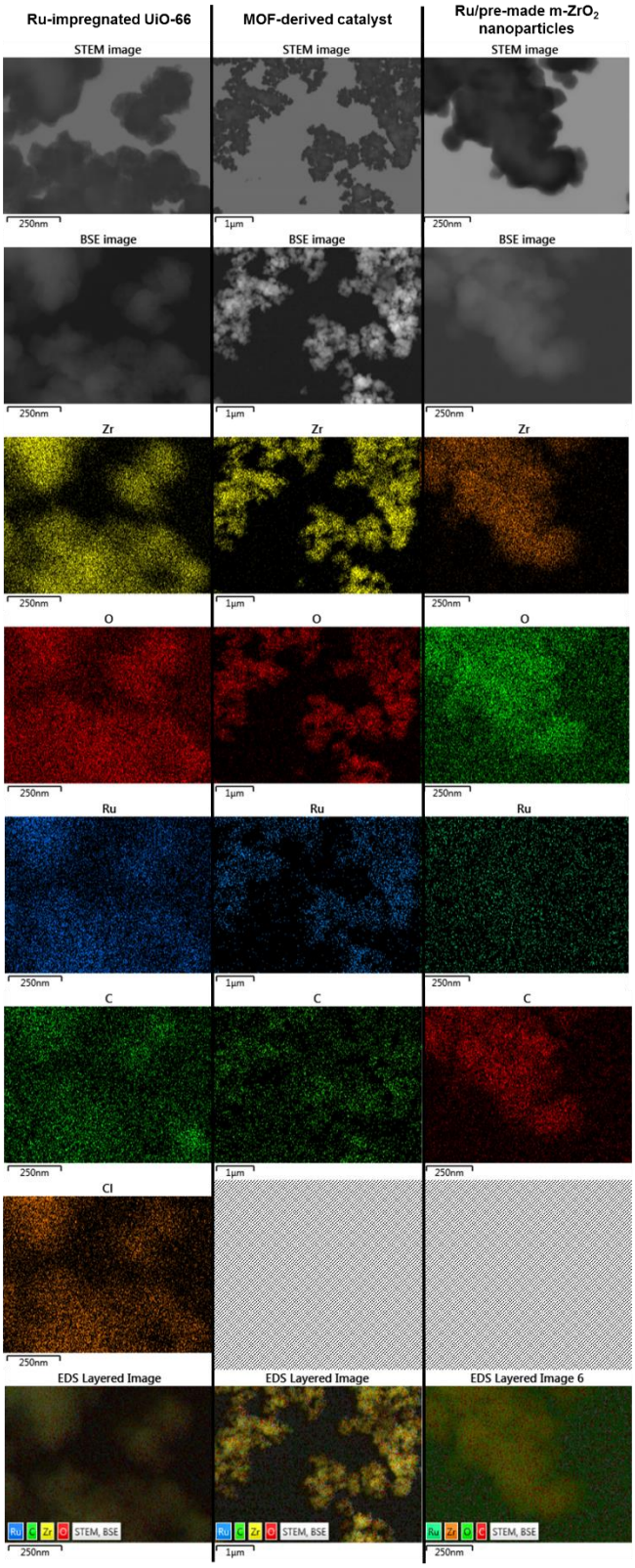

Figure S19: STEM, BSE images and EDS mapping of **1Ru/UiO-66** pre-reduced in a tube furnace at 250 °C in 5% H2-N2 for 4 hours, UiO-66 framework was retained and confirmed by XRD (**Figure S9**) (left); MOF-derived catalyst activated at 350 °C and 30 bar (centre); and Ru/pmZrO2, Ru on premade m-ZrO_2, tested at 350 °C and 30 bar (right). The comparison of these images indicate a homogeneous dispersion of ruthenium chloride within UiO-66 prior to the catalyst activation. The MOF-derived catalyst also contains Ru evenly dispersed, but no evidence of chloride. Lastly, Ru on pre-made m-ZrO_2 nanoparticles does not presents the same level of Ru dispersion over the ZrO_2 particles.

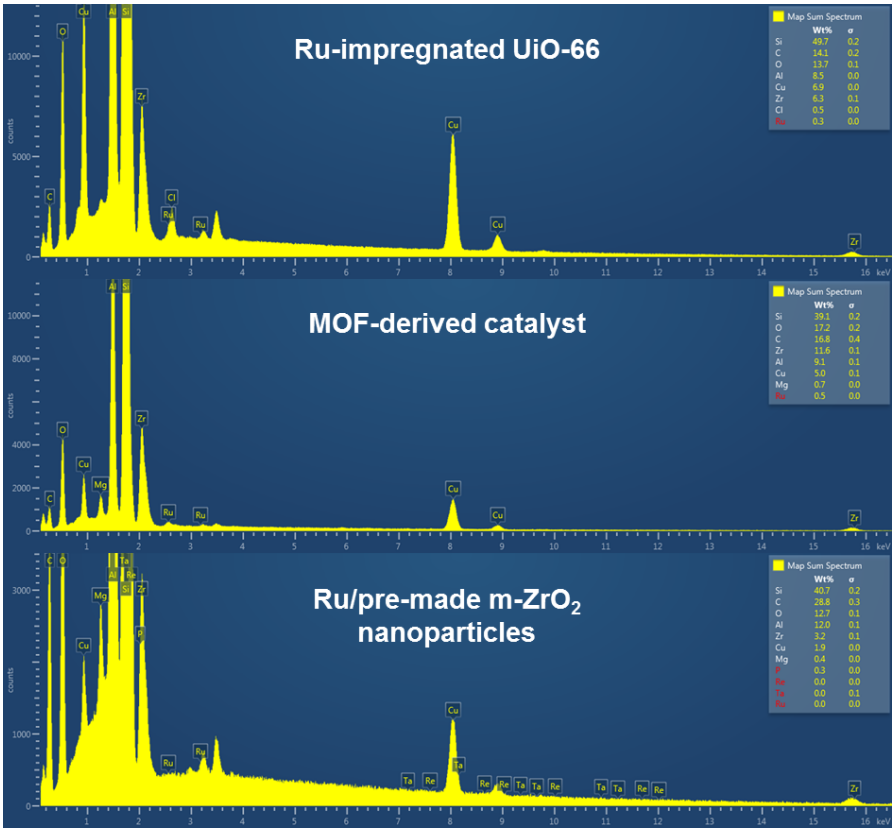

Figure S20: EDS quantitative elemental analysis for the mapping displayed in **Figure S19**.

Table S5: EDS Map Sum Spectrum quantitative analysis of MOF-derived catalyst from **Figure S20**.

Element	Wt %	σ
Si	39.1	0.2
O	17.2	0.2
C	16.8	0.4
Zr	11.6	0.1
Al	9.1	0.1
Cu	5.0	0.1
Mg	0.7	0.0
Ru	0.5	0.0

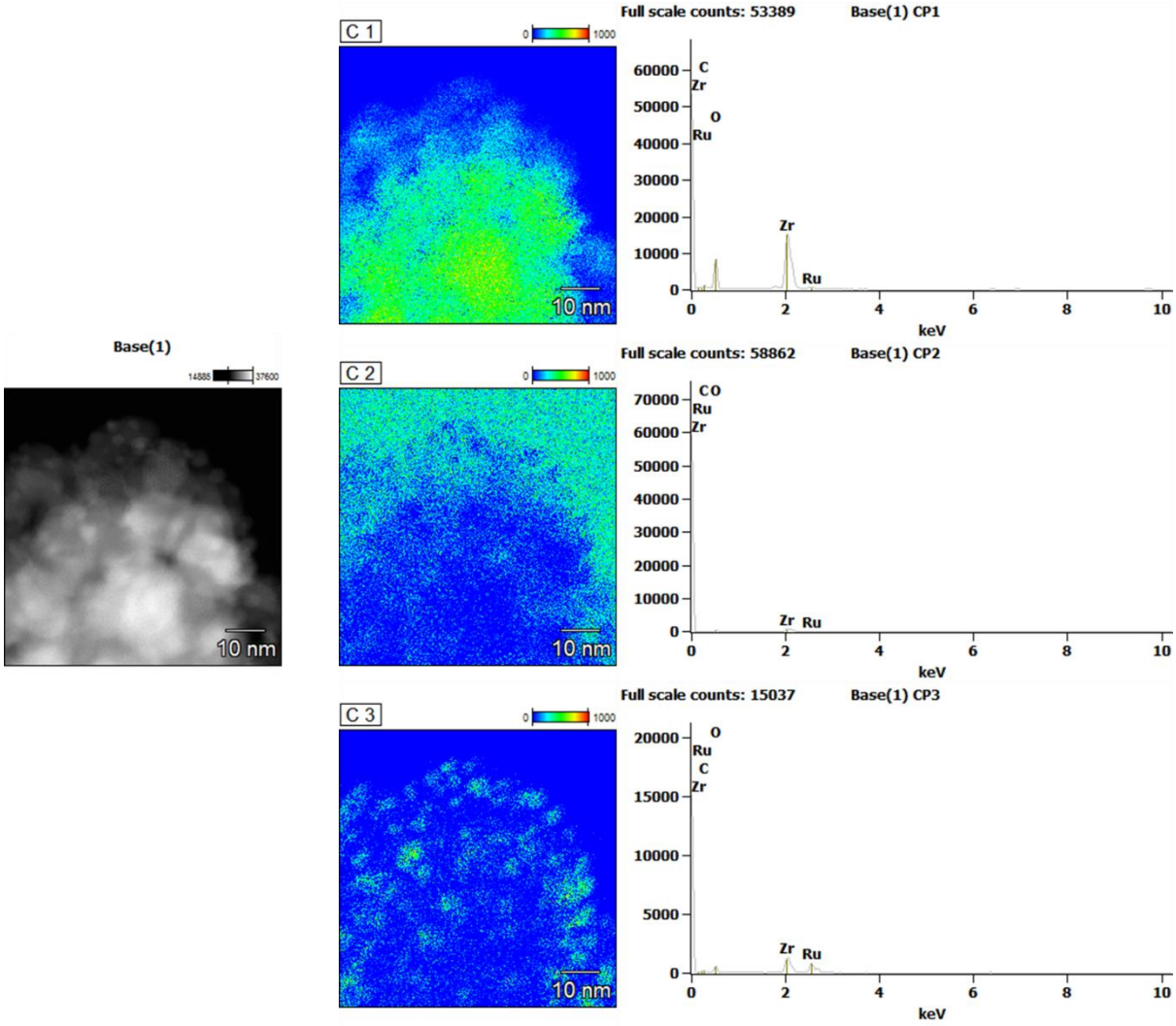

Figure S21: Compass analysis (multivariate statistical analysis) was used to separate the EDS data into regions with similar spectra. The analysis indicated 3 regions: Map C1 comprises the majority of the observable sample, C2 covers the background (sample-free region) and C3 highlights the Ru nanoparticles. Quantitative analysis of each area is shown below (**Table S6**)

Table S6: Quantitative analysis of the spectra shown in **Figure S21**. Map C3 indicated a much higher content of Ru compared to the other maps. In addition, the low O content in this map indicates Ru metal.

Map	C 1		C 2		C 3	
Element line	Wt.%	Error	Wt.%	Error	Wt.%	Error
C K	3.94	± 0.11	5.81	± 0.35	5.4	± 0.35
O K	31.31	± 0.21	21.75	± 0.59	18.59	± 0.37
Zr K	61.93	± 0.77	62.52	± 3.30	41.96	± 1.60
Ru L	2.82	± 0.11	9.92	± 0.50	34.05	± 0.70

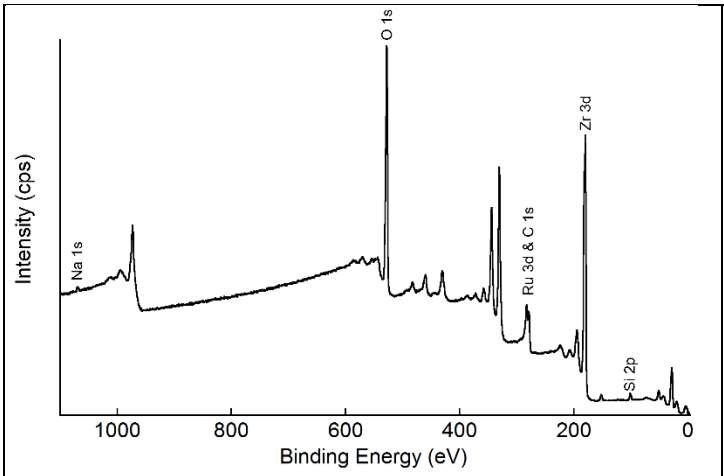

Figure S22: Selected, representative survey spectrum by XPS of the MOF-derived catalyst activated at 350 °C and 30 bar.

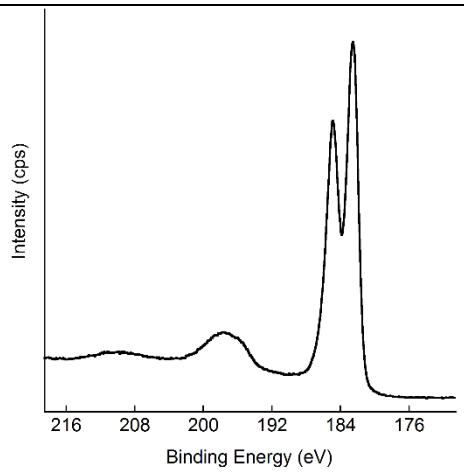

Figure S23: Selected, representative Zr 3d spectrum by XPS of the MOF-derived catalyst activated at 350 °C and 30 bar.

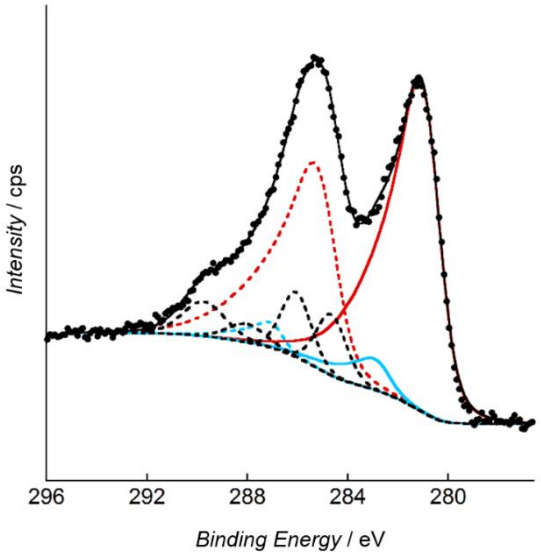

Figure S24: Selected, representative high resolution spectrum of the C 1s and Ru 3d region for the MOF-derived catalyst activated at 350 °C and 30 bar by XPS. Component assignments and fit parameters are provided in Table S7.

Table S7: XPS binding energies and fit parameters for MOF-derived catalyst activated at 350 °C.

BE (eV)	Component	Peak	Peak assignment	CasaXPS fitting parameter
280.7	Red (solid)	Ru 3d5/2	RuO2	LF(0.25,1,45,280)
284.9	Red (dashed)	Ru 3d3/2		LF(0.25,1,45,280)
282.6	Blue (solid)	Ru 3d5/2 sat	RuO2 satellite	LF(0.25,1,45,280)
286.8	Blue (dashed)	Ru 3d3/2 sat		LF(0.25,1,45,280)
284.7	Black (dashed)	C 1s	C-C, C-H	GL(30)
286	Black (dashed)	C 1s	C-O	GL(30)
287.9	Black (dashed)	C 1s	O-C-O, C=O	GL(30)
289.5	Black (dashed)	C 1s	CO2R, CO3	GL(30)

Table S8: Elemental composition of the MOF-derived catalyst activated at 350 °C and 30 bar by XPS.

Element	Mean Atomic%	Std. dev
O	53.75	1.96
Zr	23.97	1.66
C	15.74	0.16
Si	3.34	0.13
Ru	2.82	0.02
Na	0.38	0.01

References

1 M. J. Katz, Z. J. Brown, Y. J. Colón, P. W. Siu, K. a. Scheidt, R. Q. Snurr, J. T. Hupp and O. K. Farha, *Chem. Commun.*, 2013, **49**, 9449-9451.

2 V. Meynen, P. Cool and E. F. Vansant, *Microporous Mesoporous Mater.*, 2009, **125**, 170-223.

3 B. Schmitt, C. Bronnimann, E. F. Eikenberry, F. Gozzo, C. Hormann, R. Horisberger and B. Patterson, *Nucl. Instrum. Methods Phys. Res., Sect. A*, 2003, **501**, 267-272.

4 *Journal*, 2012.

5 A. J. Gerbasi da Silva, P. Claassens-Dekker, A. C. Sallarès de Mattos Carvalho, A. Manzolillo Sanseverino, C. Pontes Bittencourt Quitete, A. Szklo and E. Falabella Sousa-Aguiar, *J. Environ. Chem. Eng.*, 2014, **2**, 2148-2155.

6 J. K. van der Waal, G. Klaus, M. Smit and C. M. Lok, *Catal. Today*, 2011, **171**, 207-210.

7 J. J. Gao, Y. L. Wang, Y. Ping, D. C. Hu, G. W. Xu, F. N. Gu and F. B. Su, *RSC Adv.*, 2012, **2**, 2358-2368.

8 M. Kurth and P. C. J. Graat, *Surf. Interface Anal.*, 2002, **34**, 220-224.

9 G. Beamson and D. Briggs, *High Resolution XPS of Organic Polymers: The Scienta ESCA300 Database*, Wiley, 1992.

10 A. Lyapin and P. C. J. Graat, *Surf. Interface Anal.*, 2004, **36**, 812-815.

11 A. Lyapin, L. P. H. Jeurgens, P. C. J. Graat and E. J. Mittemeijer, *Surf. Interface Anal.*, 2004, **36**, 989-992.

12 A. E. Hughes, in *Mater. Sci. Monogr.*, ed. N. Janusz, Elsevier, 1995, vol. Volume 81, pp. 183-238.

13 D. J. Morgan, *Surf. Interface Anal.*, 2015, **47**, 1072-1079.

14 J. M. Soler, E. Artacho, J. D. Gale, A. García, J. Junquera, P. Ordejón and D. Sánchez-Portal, *J. Phys.: Condens. Matter*, 2002, **14**, 2745-2779.

15 J. P. Perdew, K. Burke and M. Ernzerhof, *Phys. Rev. Lett.*, 1996, **77**, 3865-3868.

16 H. Barron, L. Fernández-Seivane and X. López-Lozano, *physica status solidi (b)*, 2014, **251**, 1239-1247.

17 H. Barron, L. Fernández-Seivane, H. C. Weissker and X. López-Lozano, *J. Phys. Chem. C*, 2013, **117**, 21450-21459.

18 L. Valenzano, B. Civalleri, S. Chavan, S. Bordiga, M. H. Nilsen, S. Jakobsen, K. P. Lillerud and C. Lamberti, *Chem. Mater.*, 2011, **23**, 1700-1718.